Unconventional quantum fluid at high magnetic fields in the marginal charge-density-wave system α-(BEDT-TTF)$_2M$Hg(SCN)$_4$ (M=K and Rb)

N. Harrison,[1] J. Singleton,[1] A. Bangura,[2] A. Ardavan,[2] P. A. Goddard,[1,2] R. D. McDonald,[1] and L. K. Montgomery[3]
[1]*National High Magnetic Field Laboratory, LANL, MS-E536, Los Alamos, New Mexico 87545, USA*
[2]*The Clarendon Laboratory, Parks Road, Oxford OX1 3PU, United Kingdom*
[3]*Department of Chemistry, Indiana University, Bloomington, Indiana 47405, USA*
(Received 15 November 2003; revised manuscript received 16 January 2004; published 5 April 2004)

Single crystals of the organic charge-transfer salts α-(BEDT-TTF)$_2M$Hg(SCN)$_4$ have been studied using Hall-potential measurements (M=K) and magnetization experiments (M=K, Rb). The data show that two types of screening currents occur within the high-magnetic-field, low-temperature charge-density wave (CDW$_x$) phases of these salts in response to time-dependent magnetic fields. The first, which gives rise to the induced Hall potential, is a free current ($\mathbf{j}_{\rm free}$), present at the surface of the sample. The time constant for the decay of these currents is much longer than that expected from the sample resistivity. The second component of the current appears to be magnetic ($\mathbf{j}_{\rm mag}$), in that it is a microscopic, quasiorbital effect; it is evenly distributed within the bulk of the sample upon saturation. To explain these data, we propose a simple model invoking a new type of quantum fluid comprising a CDW coexisting with a two-dimensional Fermi-surface pocket which describes the two types of current. The model and data are able to account for the body of previous experimental data which had generated apparently contradictory interpretations in terms of the quantum Hall effect or superconductivity.

DOI: 10.1103/PhysRevB.69.165103 PACS number(s): 71.45.Lr, 71.20.Ps, 71.18.+y

I. INTRODUCTION

In their rudimentary form, charge-density waves (CDWs) constitute a simple one-dimensional spin singlet ground state in which the collective mode consists of a charge density modulated at a characteristic wave vector $Q=2k_{\rm F}$. Here, $k_{\rm F}$ is the Fermi wave vector of the Fermi-surface section responsible for CDW formation.[1–3] Compared to superconductors, their behavior in a magnetic field is relatively easy to predict, providing perhaps the simplest example of a singlet ground state reaching the Pauli limit.[4–7] This limit is defined as the magnetic field required to cause the energy of the partially spin-polarized normal state to become lower than that of the condensate.

In spite of the simplicity of CDW systems, the large values of the CDW condensation temperatures $T_{\rm p}$, typically of the order of 100 K,[1,2] make the Pauli limit inaccessible in standard laboratory magnetic fields for the vast majority of CDW materials.[8] Our reason for studying the title compounds, α-(BEDT-TTF)$_2M$Hg(SCN)$_4$, is that they lie at the far lower end of the spectrum of transition temperatures, with $T_{\rm p}\approx 8$ K (Ref. 9) for M=K and $T_{\rm p}\approx$ 12 K for M=Rb, making them perhaps the most marginal of CDW systems. Consequently, they are the only CDW compounds in which the gap is sufficiently low for the primary CDW phase, CDW$_0$, to have been shown to be Pauli limited by a relatively modest magnetic field of $\mu_0 H\approx 23$ T for M=K and $\mu_0 H\approx 32$ T for M=Rb.[6,7,10–12]

It must be stated, however, that the marginal CDW properties of α-(BEDT-TTF)$_2M$Hg(SCN)$_4$ render it somewhat beyond the predictive power of the standard theory.[4] For instance, the low transition temperature results in a CDW with a weak charge modulation that is vulnerable to fluctuations and sample-dependent effects.[9] Furthermore, the presence of large sections of the Fermi surface left ungapped by the CDW order[13] (see Fig. 1, Refs. 13–16) causes the energy associated with the coupling of the magnetic field to orbital degrees of freedom of the itinerant electrons to rival the condensation energy. This leads to a modification of the quantum oscillatory effects[7,17,18] and to the possibility of field-induced CDW subphases.[5,19]

At magnetic fields above the Pauli paramagnetic limit, α-(BEDT-TTF)$_2M$Hg(SCN)$_4$ then crosses over into a new regime in which the transition temperature becomes even lower,[10–12] falling to between 2 and 4 K: a schematic of the phase diagram is shown in Fig. 2. Since the conventional CDW phase, CDW$_0$, is no longer stable at high magnetic fields, the spin-up and spin-down electrons must instead form independent charge and spin modulations with momentum vectors $Q_\uparrow$ and $Q_\downarrow$,[5,6] leading to a different type of CDW phase.

Experimental studies of this high-magnetic-field phase, denoted CDW$_x$, lead one to question whether it is a CDW at all. While conventional wisdom has it that CDWs constitute a class of narrow-gap insulator,[1,2] experimental studies find behaviors that are reminiscent either of the quantum Hall effect[20–24] or superconductivity.[12,25–27] These experimental findings include a sharp drop in the electrical resistivity at low temperatures, persistent currents and unusual Hall-voltage phenomena. Problems arise because the quantum Hall effect[28] and superconductivity[29] have fundamentally different origins. If one attempts to categorize interpretations of experimental data in terms of the quantum Hall effect[30] or superconductivity,[25] one obtains two sets of conclusions that are in contradiction.

The present paper seeks to reconcile the body of experi-

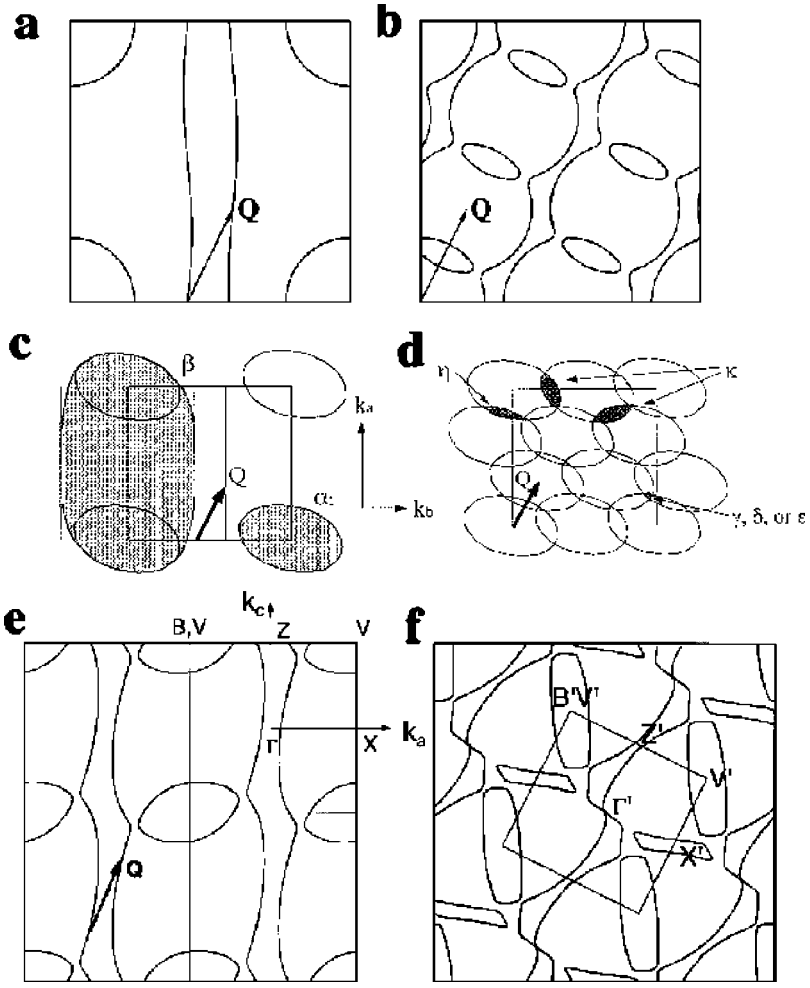

FIG. 1. A summary of models of the Fermi surface of α-(BEDT-TTF)$_2$KHg(SCN)$_4$ before and after reconstruction due to CDW$_0$ formation. (a) depicts the earliest Fermi-surface calculation (Ref. 14). If the quasi-one-dimensional sections are assumed to nest perfectly with a nesting vector **Q**, one obtains a reconstructed Fermi surface of the form shown in (b) (Ref. 15). (c) shows a notional model of the Fermi surface from Ref. 16; nesting of the one-dimensional sheets is perfect, giving rise to the network of interconnected ellipses in (d). (e) shows a Fermi-surface model in which the transfer integrals of the tight-binding Hamiltonian were fitted to a wide range of experimental data (Ref. 13). Imperfect, commensurate nesting gives rise to the reconstructed Fermi surface shown in (f). Note that the nesting vector **Q** of the model shown in (e) and (f) is in reasonable agreement with structural studies (Ref. 9). Evidence for a reconstructed Fermi surface within the proposed CDW$_x$ phase (see Fig. 2) has not as yet been reported, preventing estimates of the nesting vector from being made. One possibility is that the reduced CDW gaps in the CDW$_x$ phase allow quasiparticles to easily tunnel through them at high magnetic fields. Complete magnetic breakdown would then account for the comparatively large amplitude of the quantum oscillations of the α frequency observed within that phase (Ref. 13).

mental evidence[12,20–27] in exploring the predicted properties of a new type of quantum fluid, consisting of a CDW coexisting with a two-dimensional (2D) Fermi surface. A simple model shows that the exchange of quasiparticles between these subsystems results in the sample partially screening time- and spatially varying electromagnetic fields via two types of current flow; this result is supported by the experimental data in this work, which show that the screening currents observed in earlier magnetic measurements[12,20,26,27,33] comprise two parts. The first is weighted mostly towards the sample edges and can be considered a free current $\mathbf{j}_{\rm free}$, furnishing a Hall-potential gradient. The second contribution is analogous to the ''magnetic currents'' $\mathbf{j}_{\rm mag}$ used to represent the effects of localized orbital moments[31] in producing magnetization. These currents, which are essentially of infinite duration,[12] represent a local, microscopic current flow within the bulk of the sample; they occur if the surface screening mechanism fails, causing the CDW, instead, to be coerced by an external change in magnetic field into a nonequilibrium state. In this case, bulk currents are supported by CDW pinning forces and are not free.

The remainder of this paper is organized as follows. Experimental details are given in Sec. II, while Sec. III describes the Hall potential measurements which characterize the surface current density $\mathbf{j}_{\rm free}$. The ''magnetic'' current density $\mathbf{j}_{\rm mag}$ is studied using torque magnetometry in Sec. IV. Conclusions are given in Sec. V; for ease of reference, the model describing the microscopic mechanism that leads to $\mathbf{j}_{\rm free}$ and $\mathbf{j}_{\rm mag}$ is described in the Appendix.

II. EXPERIMENT

The free electrical current distribution, $\mathbf{j}_{\rm free}$, is determined using the variant of the Corbino geometry described in Ref. 24 in which pairs of small graphite-paint contacts are placed on the outer edge and upper surface of a α-(BEDT-TTF)$_2$KHg(SCN)$_4$ sample. Currents are induced in the sample by applying a small sinusoidal oscillatory field of amplitude $\mu_0\tilde{H}$ and angular frequency ω superimposed on the quasistatic field $\mu_0 H$ provided by a 33 T Bitter coil at NHMFL, Tallahassee. Alternatively, currents are induced by sweeping the quasistatic field at a rate $\mu_0(\partial H/\partial t)$. Provided that the sample dimensions are much smaller than its skin depth (so that it is entirely penetrated by the changing field), the resulting Hall potential between the edge of the sample, of area A, and its geometrical center is[24]

$$V_{\rm H}=\frac{A}{4\pi}\left(\frac{\rho_{xy}}{\rho_{||}}\right)\mu_0\frac{\partial H}{\partial t} \quad \text{(swept field)}, \tag{1}$$

and

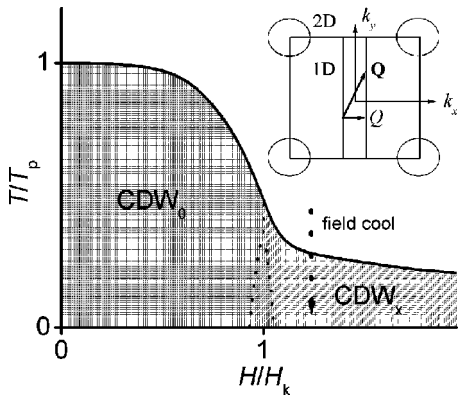

FIG. 2. Charge-density-wave formation in α-(BEDT-TTF)$_2M$Hg(SCN)$_4$ salts. A schematic of the phase diagram as a function of reduced temperature T/T_p and reduced magnetic field H/H_k (based on Ref. 25). The second-order transition temperature T_p at $H=0$ is ≈ 8 K in the $M=$ K salt and 12 K in the $M=$ Rb salt. Likewise, the first-order ''kink'' transition field $\mu_0 H$ at $T=0$ (roughly corresponding to the Pauli paramagnetic limit), is 23 T for $M=$K and 32 T for $M=$Rb. 'CDW$_0$' refers to the proposed conventional CDW phase while CDW$_x$ refers to an incommensurate phase that comes into existence at high magnetic fields. The inset shows a simplified model of the Fermi surface in the repeated Brillouin zone representation (after Ref. 30). This consists of open one-dimensional (1D) sections which run along k_y and a closed 2D section; it is used in the derivations given in the Appendix. (More accurate representations of the Fermi surface topology are given in Fig. 1.) CDW formation is thought to occur for a characteristic ''nesting vector'' **Q** (Ref. 13) (with a component Q along k_x), causing the 1D section to become gapped.

$$V_H = \frac{A}{4\pi}\left(\frac{\rho_{xy}}{\rho_{||}}\right)\omega\mu_0\tilde{H} \qquad \text{(oscillatory field)}, \tag{2}$$

where $\rho_{||}$ is an appropriate average of ρ_{xx} and ρ_{yy} and standard symbols for the components of the resistivity tensor are used.

Under the conditions of almost complete penetration by the oscillatory field, the phase of V_H in Eq. (2) with respect to $\tilde{H}$ is the same as that of a voltage induced in an open loop (i.e., $\pi/2$). However, if significant screening occurs, V_H will also contain a component in quadrature to this. Using standard complex notation, we write

$$V_H = V_H' - iV_H'', \tag{3}$$

where V_H' and V_H'' are the dissipative and reactive (quadrature) components of V_H, respectively. In our experiment, phase-sensitive detection techniques allow V_H' and V_H'' to be simultaneously recorded for analysis purposes; the signal from a multiturn pick-up coil mounted close to the sample is used to define the *real* phase. The approximate distribution of the current is further determined by placing pairs of contacts arranged between the outer and upper surfaces of the sample of α-(BEDT-TTF)$_2$KHg(SCN)$_4$ of volume ≈ 1 mm^3 shown in Fig. 3. While the finite size of 100 ± 50 μm of the electrical contacts applied using graphite paint limit the spatial resolution of the experiment, the contacts do enable one to distinguish between different models.

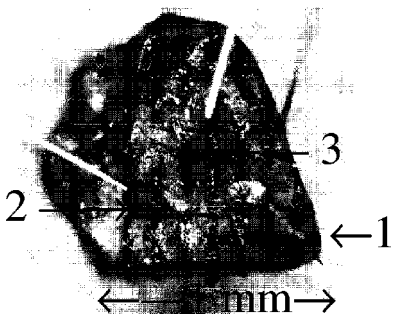

FIG. 3. A photograph of the sample of α-(BEDT-TTF)$_2$KHg(SCN)$_4$ used in the measurements of the Hall potential, showing three contacts on the upper surface of the sample. Contacts on the side are not in focus.

During these experiments, temperatures down to 0.5 K are achieved using a plastic ^{3}He refrigerator.

The orbital magnetic currents, $\mathbf{j}_{mag}$, are determined by measuring the magnetic torque of a different $M=$K sample to that shown in Fig. 3 as well as a $M=$ Rb sample. In each case, θ, the angle between the magnetic field **H** and the normal to the sample's conducting planes is restricted to small angles ($\theta \leqslant 20°$); this avoids complications due to magnetic torque interaction.[30] The torque is measured capacitively by attaching the sample to a 5-μm-thick phosphor-bronze cantilever that forms one of the plates of a capacitor. Electrical contacts applied to the sample confirm that $\mathbf{j}_{mag}$ continues to persist after the electrical currents dissipate. In these experiments, temperatures down to 50 mK are provided by a dilution refrigerator.

III. HALL POTENTIAL MEASUREMENTS

Figure 4 shows typical measured Hall potentials V_H' and V_H'' due to an oscillatory field; in this case $\mu_0\tilde{H}=2.6$ mT, $\omega/2\pi=409.6$ Hz and the temperature of the α-(BEDT-TTF)$_2$KHg(SCN)$_4$ sample ($A\approx 1.1$ mm^2) is 0.5 K. The V_H data in Fig. 4 correspond to the contact labeled 3 in Fig. 3; as the contact on the upper face of the sample is very near to its geometrical center, we expect that the Hall potential will be close to the maximum value possible. Note that there is a small field-independent inductive

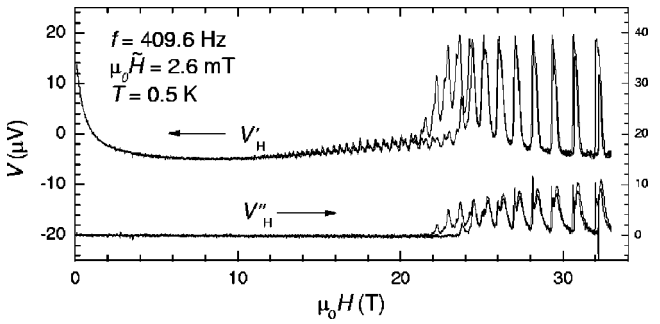

FIG. 4. Examples of the real and imaginary Hall potentials V_H' and V_H'' measured with the third pair of contacts on the sample shown in Fig. 3. An oscillatory applied field with $\mu_0\tilde{H}\approx 2.6$ mT rms and $\omega/2\pi=409.6$ Hz is used; $T\sim 0.5$ K. Arrows indicate the axis corresponding to each data set.

pickup contribution $V_{\rm pu}$ to $V_{\rm H}'$ due to the open-loop area ($\lesssim 1$ mm^2) between the contacts. By comparing measured $V_{\rm H}'$ values at several different fields, it is possible to infer that $V_{\rm pu} \approx -4.7$ μV.

In the discussion that follows, we first attempt to analyze the data of Fig. 4 in terms of conventional bulk currents within the *whole* of the α-(BEDT-TTF)$_2$KHg(SCN)$_4$ sample; the analysis uses conductivity and resistivity tensor elements which do not vary spatially. We shall find that while this conventional analysis describes the behavior of $V_{\rm H}'$, albeit with some remarkably low values of $\rho_{||}$, it is unable to account for the variation of $V_{\rm H}''$ with H.

A. Analysis in terms of bulk currents

In a reasonably isotropic quasi-two-dimensional metal, the components of the resistivity (ρ) and conductivity (σ) tensors are related by the expressions

$$\rho_{xy} = \frac{\sigma_{xy}}{\sigma_{||}^2 + \sigma_{xy}^2}, \qquad \rho_{||} = \frac{\sigma_{||}}{\sigma_{||}^2 + \sigma_{xy}^2}. \tag{4}$$

Thus, the ratio $\rho_{xy}/\rho_{||}$ in Eq. (2) is equivalent to $\sigma_{xy}/\sigma_{||}$; it is therefore likely that the asymptotic variation of $V_{\rm H}'$ at low fields is due to the divergence of

$$\sigma_{xy} = \varrho_{\rm 2D}/\mu_0 H, \tag{5}$$

where $\varrho_{\rm 2D}$ is the charge density of the 2D holes, as $H \to 0$.

As H increases, $\rho_{xy}/\rho_{||}$ becomes smaller, leaving $V_{\rm pu}$ as the dominant contribution to the measured $V_{\rm H}'$. However, after the ''kink'' transition at $\mu_0 H \approx 23$ T, $V_{\rm H}'$ undergoes a resurgence and the quadrature component $V_{\rm H}''$ becomes significant for the first time. The maxima in $V_{\rm H}'$ occur at integral Landau level filling factors $\nu = F/\mu_0 H$, where F is the magnetic quantum oscillation frequency; at such fields, the chemical potential μ is situated in a Landau gap. The peak values $V_{\rm H}' \approx 25$ μV (at $\mu_0 H \approx 25$ T) correspond to $\rho_{xy}/\rho_{||} \approx 42$; the fact that $\rho_{xy} \gg \rho_{||}$ allows us to use $\rho_{xy} \approx 1/\sigma_{xy} = \mu_0 H/\varrho_{\rm 2D}$ [see Eq. (5)] with $\varrho_{\rm 2D}/e = 1.6 \times 10^{26}$ m^{-3} (Ref. 30) to extract a minimum sample resistivity of $\rho_{||} \approx 2.4 \times 10^{-8}$ Ωm. Such resistivity values are characteristic of a good metal at room temperature and are not too dissimilar from the results of ac susceptibility experiments on α-(BEDT-TTF)$_2$KHg(SCN)$_4$.[33]

To examine the apparent bulk resistivity components in more detail, we rearrange Eqs. (4) in terms of $\rho_{||}/\rho_{xy}$ and σ_{xy} to yield

$$\rho_{xy} = \frac{1}{\sigma_{xy}\left[1 + \left(\frac{\rho_{||}}{\rho_{xy}}\right)^2\right]} \tag{6}$$

and

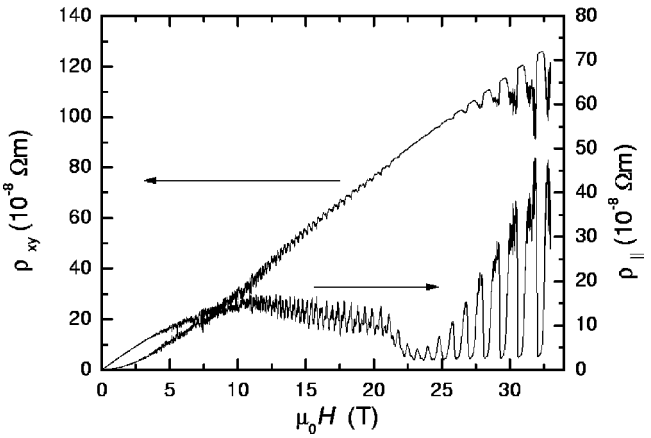

FIG. 5. The bulk resistivity tensor elements ρ_{xy} and $\rho_{\|}$ estimated from $V_{\rm H}'$ using Eqs. (6) and (7) ($T = 0.50$ K). Arrows indicate the axis corresponding to each data set.

$$\rho_{\|} = \frac{\left(\frac{\rho_{\|}}{\rho_{xy}}\right)}{\sigma_{xy}\left[1 + \left(\frac{\rho_{\|}}{\rho_{xy}}\right)^2\right]}. \tag{7}$$

These equations can then be used along with Eqs. (2) and (5) to convert the experimental values of $V_{\rm H}'$ to apparent bulk in-plane resistivity components.

The results of this procedure are shown in Fig. 5; the linear increase of ρ_{xy} with H and quadratic increase of $\rho_{\|}$ with H at low magnetic fields show that the method gives a behavior in accord with expectations. At higher fields, the deduced values of ρ_{xy} behave in a similar manner to earlier direct measurements of oscillations in the Hall resistivity.[22] However, it is interesting to note that the in-plane resistivity is lower in Fig. 5 than that obtained from four-terminal methods.[22] Owing to nonuniform current flow associated with sample imperfections, direct measurements of the in-plane resistivity are often contaminated by the interplane component ρ_{zz}, which is several orders larger in magnitude.[22]

The unusually large value of $\rho_{xy}/\rho_{\|} = 42$ and consequent low value of $\rho_{\|}$ estimated from the oscillatory field measurements are confirmed by setting $\tilde{H} = 0$ and by sweeping the quasistatic field. Data obtained using $\mu_0 \partial H/\partial t = 0.5$ T s^{-1} are shown in Fig. 6 for both rising and falling magnetic fields. Insertion of this rate of change of field into Eq. (1), along with the value $\rho_{xy}/\rho_{\|} \approx 42$ obtained in the oscillatory-field experiments (see above), yields $V_{\rm H} \approx 1.8$ μV at $\mu_0 H \approx 25$ T, in good agreement with the data shown in Fig. 6. However, the magnitude of the Hall potential continues to increase with increasing field, rising to a value of $V_{\rm H} \approx 8$ μV at around 32 T (Fig. 6). This yields $\rho_{xy}/\rho_{\|} = 180$, corresponding to $\rho_{\|} \approx 6 \times 10^{-9}$ Ωm, which is several times lower than the resistivity of room-temperature copper. Such values for these parameters would not be unusual for a two-dimensional electron gas exhibiting the quantum Hall effect.[28] However, they are unusual for a bulk organic metal far from the quantum limit, for example, $\nu \approx 21$ at 32 T.

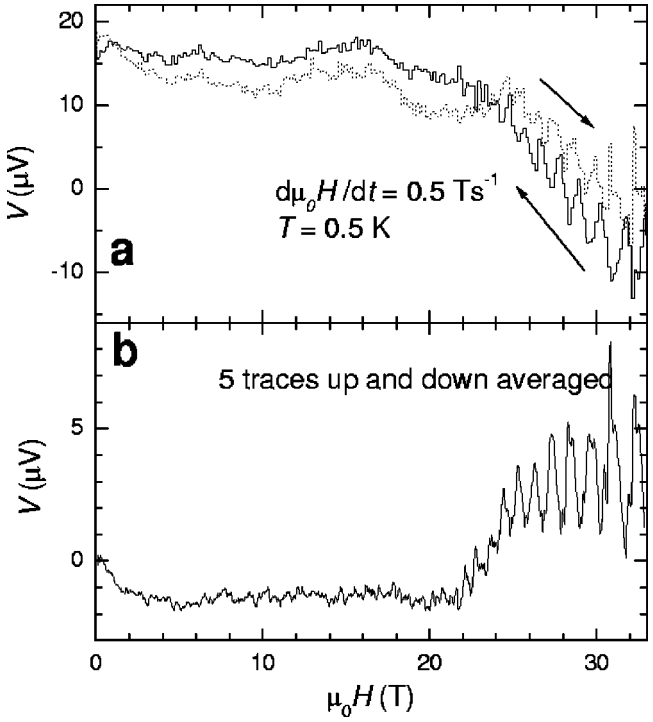

FIG. 6. An example of the Hall potential V_H measured for the third pair of contacts in a slowly varying magnetic field (sweep rate $\partial\mu_0 H/\partial t = 0.5$ Ts^{-1}; $T = 0.50$ K). (a) shows raw data for a single sweep, with arrows indicating the sweep direction. No filtering has been applied. The background nonoscillatory component could be caused by variations in the contact potentials with magnetic field. (b) The difference $(V_{H,up} - V_{H,down})/2$ between rising- and falling-magnetic-field data averaged over 5 sweeps.

B. Analysis in terms of edge currents

Thus far, a conventional treatment employing uniform conductivity tensor elements $\sigma_\parallel$ and σ_{xy} has given an *apparently* satisfactory explanation of the Hall potential measured in swept fields and the real component of the Hall potential V'_H observed in oscillatory fields, albeit with extremely low values of the bulk resistivity. However, this simple model fails on considering the imaginary component V''_H which appears within the high magnetic field regime in Fig. 4. Were α-(BEDT-TTF)$_2$KHg(SCN)$_4$ a conventional metal, then in order to have a quadrature component of the order of 30% of the in-phase component at $\omega/2\pi = 409.6$ Hz, the skin depth must be comparable to or shorter than the effective radius $r_0 = \sqrt{A/\pi} \sim 590$ μm of the sample.[34] If we estimate the skin-depth $\delta = \sqrt{2\rho_\parallel/\mu_0\omega}$ from the above resistivity value ($\rho_\parallel \sim 2.4\times10^{-8}$ Ωm), however, we obtain a value $\delta = 3.9$ mm that is significantly greater than the sample size. The presence of a large finite V''_H term, therefore, cannot be easily explained by a simple conductivity tensor model.

A further indication of the fact that the induced currents do not obey a conventional bulk mechanism is given by using the contact arrangements shown in Fig. 3 to explore the dependence of V'_H and V''_H on the distance d of the contact on the upper surface of the sample from the edge. For a spatially homogeneous metallic system in a slowly time-varying magnetic field, it is trivial to show that the current density and concomitant Hall potential should vary quadratically,

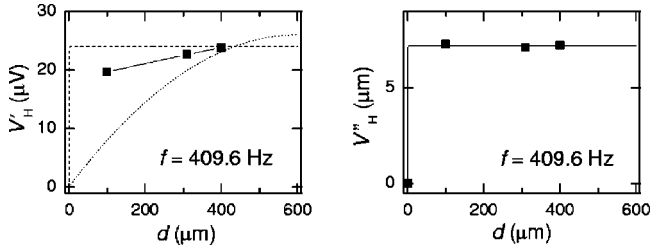

FIG. 7. The Hall potential difference between the edge and a voltage probe situated a distance d inside the upper surface where $d = 100$, 310, and 400 μm for contacts 1, 2, and 3, respectively, with $T = 0.5$ K, $f = 409.6$ Hz, and $\mu_0\tilde{H} = 2.6$ mT. Left: the normal Hall voltage V'_H; the dotted line shows the voltage distribution expected according to Eq. (8) while the dashed line shows the voltage distribution expected for an exponential variation of the Hall potential, $V_H \propto \exp(-d/\lambda)$. Right: the reactive Hall voltage V''_H, with the solid line depicting $V_H \propto \exp(-d/\lambda)$ with $\lambda \ll 100$ μm.

$$V_H(d) = \frac{d(2r_0 - d)}{r_0^2}\, V_{H,max}, \tag{8}$$

where $V_{H,max}$ is the total potential difference between the outer surface and geometric center of the sample. This form occurs because the size of the area loop element susceptible to induced voltages increases parabolically with the distance from the geometric center of the sample. On comparing the detected Hall potentials for the three different contact arrangements shown in Fig. 3, we find that V'_H at $\mu_0 H \approx 25$ T in Fig. 7 varies more slowly with d than predicted by Eq. (8). In the case of the reactive component, no discernable dependence of V''_H on d is seen. This type of behavior shows that the Hall potential difference (and therefore also the current) is heavily weighted towards the sample edge, with the effect being particularly pronounced for the imaginary component.

Currents carried at or close to the edge are expected to occur in quantum-Hall-effect systems for which $\sigma_\parallel \to 0$ at integral Landau-level filling factors. These currents are either carried within edge channels,[28] giving rise to a kind of chiral Fermi liquid,[35] or are bulk states near the edge in which electrostatic forces locally deplete (or enhance) the charge carrier density.[36] Were a situation where $\sigma_\parallel \to 0$ realized in α-(BEDT-TTF)$_2$KHg(SCN)$_4$, perfect screening would give rise to a Hall potential that is entirely reactive, even in the limit as $\omega \to 0$. Experimentally, $|V''_H/V'_H| \lesssim 1$, implying two things: first $\sigma_\parallel \neq 0$ within the bulk and second the partial screening that takes place has to occur within a region around the perimeter of the sample that is thinner than the bulk skin depth.

In the Appendix, we show that a system comprising a CDW coexisting with quasi-two-dimensional Landau levels can lead to very effective screening currents within a distance $\lambda = \sqrt{m/2\mu_0 e\varrho_{2D}}$ of the sample surface. Although the finite size of the electrical contacts in Fig. 3 (100 ± 50 μm in diameter), limits the resolution to which we can analyze the

Hall voltage distribution in Fig. 7, we can, nevertheless, perform some simple consistency checks on this model. We propose that all of the current flows within a distance λ of the surface of the sample, and that this current flow encounters a characteristic (very low) resistivity ρ_λ. The system is like an LR (inductance-resistance) circuit, with

$$L=\frac{\alpha\mu_0\pi r_0^2}{l} \tag{9}$$

and

$$R=\frac{2\pi r_0\rho_\lambda}{\lambda l}, \tag{10}$$

where l is the sample height, $r_0=\sqrt{A/\pi}$ is its effective radius, and α is a so-called Nagaoka parameter, a numerical factor ~ 1 that depends on l/r_0.[37] For our sample, $\alpha\approx 0.5$. In a magnetic field swept at a slow uniform rate, this treatment yields

$$V_H=\frac{r_0\lambda}{2}\left(\frac{\rho_{xy}}{\rho_\lambda}\right)\mu_0\frac{\partial H}{\partial t}+V_{H0}e^{-t/t_0} \tag{11}$$

[c.f. Eq. (1)] whereas for a sinusoidally oscillating field we obtain

$$V_H=V_H'-iV_H''=\frac{r_0\lambda}{2}\left(\frac{\rho_{xy}}{\rho_\lambda}\right)\frac{\mu_0\omega\tilde{H}}{1+\omega^2t_0^2}(1-i\omega t_0). \tag{12}$$

Here

$$t_0=L/R=\alpha\mu_0 r_0\lambda/2\rho_\lambda \tag{13}$$

is a characteristic inductive decay time and $V_{H0}e^{-t/t_0}$ represents transient solutions due to rapid changes in $\partial H/\partial t$ and/or R.

We first compare Eq. (11) with the Hall potential of 8 μV observed in Fig. 6 at $\mu_0H\approx 32$ T, obtaining $\rho_\lambda/\lambda\approx 23\ \mu\Omega$, or $\rho_\lambda\approx 9\times 10^{-12}\ \Omega$m, using $\lambda\approx 400$ nm (see the Appendix). Inserting this into the semiclassical Drude expression $\rho_\lambda=m/e\varrho_{2D}\tau$, we obtain a scattering time of $\tau\approx 50$ ns, or, a mean-free-path $\Lambda=v_F\tau\approx 5$ mm (where we have obtained the Fermi velocity from $v_F=\sqrt{2\hbar eF/m}$). The fact that Λ is comparable to the sample perimeter of 4 mm could be consistent with ballistic transport. The ballistic transport regime, for which finite values of $\sigma_\parallel$ can no longer be locally defined, is one of the essential preconditions of the edge-weighted current model (see the Appendix).

Two separate estimates of t_0 can be made. First, we can rearrange Eqs. (12) and (13) to yield $t_0=\alpha V_H'(1+\omega^2t_0^2)/\rho_{xy}\omega\tilde{H}$. In the limit of low frequency, $\omega^2t_0^2\ll 1$, so that this can be written as

$$t_0^{\text{resist}}=\frac{\alpha V_H'}{\rho_{xy}\omega\tilde{H}}, \tag{14}$$

where the superscript ''resist'' denotes that this estimate of the characteristic time is derived from the dissipative (i.e., resistive) component of V_H. An alternative estimate can be made by comparing the resistive and reactive parts of V_H,

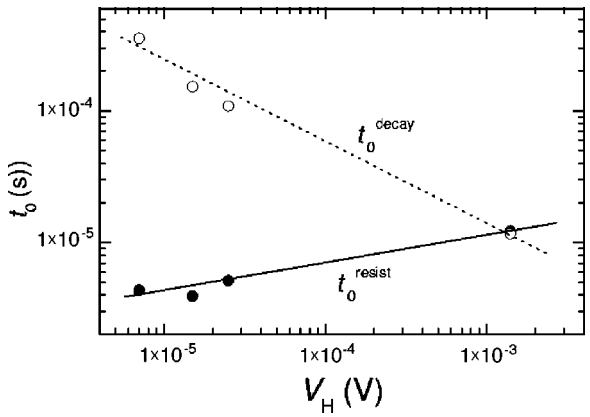

FIG. 8. A comparison of the decay times t_0^{decay} and t_0^{resist}. All estimates were made for $\mu_0H\approx 25$ T and $T=0.5$ K, with the data points corresponding to excitation frequencies $\omega/2\pi=51.25$, 208.6, 409.6, and 8809 Hz and oscillating field amplitudes $\mu_0\tilde{H}=6.51$, 3.90, 2.62, and 3.75 mT.

$$t_0^{\text{decay}}=\frac{|V_H'|}{\omega|V_H''|}, \tag{15}$$

where the superscript ''decay'' denotes that this is analogous to the technique used to find the decay time of conventional LR circuits.

Figure 8 shows t_0^{resist} and t_0^{decay} deduced from experimental data ($\mu_0H\approx 25$ T, temperature$=0.5$ K). If the sample surface layer functioned as a conventional (but high-conductivity) metal, we should expect the two times to be the same. However, the divergence between t_0^{decay} and t_0^{resist} at low frequencies, or low values of V_H, is unconventional. This suggests that the sample behaves resistively when attempting to drive a current through it, but once established, the currents have a tendency to last longer than expected for a conventional metal. Their lifetime t_0^{decay} becomes particularly long at low values of the Hall potential V_H observed in slowly varying magnetic fields.

In rapidly varying magnetic fields, t_0^{decay} converges with t_0^{resist} at $V_H\approx 1$ mV. This is similar to the saturation value of V_H observed in ms-duration pulsed magnetic fields.[24,38] Attempts to explain this saturation in terms of the breakdown of the quantum Hall effect have been largely unsuccessful owing to the enormous magnitude of the electric field that is required. An electric field that is concentrated towards the sample edge within a distance λ (see the Appendix), however, increases the probability of Zener tunneling. Moreover, the increased size of the unit cell in the CDW phase compared to the normal metallic phase makes Zener tunneling across the CDW gap more likely than Landau level tunneling. In such a model for the magnitude of the threshold electric field $E_Z=\varepsilon_g^2/ea\varepsilon_F$ (where $\varepsilon_g=2\Psi$ is the CDW gap and ε_F is the Fermi energy), the lattice periodicity $a=2\pi/Q\approx\pi/k_F$ occurs in the denominator. Assuming an exponential variation of the electric field where $V_H=\lambda E_Z$, we obtain

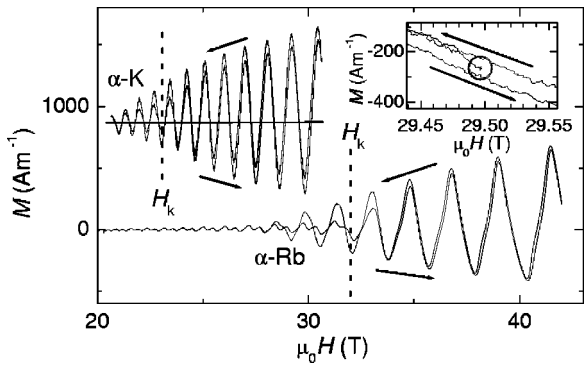

FIG. 9. The magnetization M of samples of the $M=$K ($\theta \approx 19.5°$) and Rb ($\theta \approx 5°$) salts measured on both rising and falling fields at $T=50$ mK for $M=$K and $T=0.45$ K for $M=$Rb made using the magnetic torque method. Arrows indicate the direction of sweep. For the $M=$ Rb salt, at fields below ≈ 29 T, the CDW_0 phase is stable. The region between 29 T and 33 T appears to be disturbed since H_k is different between rising and falling fields. At fields above ≈ 33 T, the transition into the CDW_x phase is complete. The de Haas-van Alphen oscillations are the same for rising and falling fields, apart from a relative offset $2\Delta M$. For the $M=$K salt, the magnetic torque shows similar features to that measured in Ref. 12. The inset shows the magnetization measured after a field cool (as indicated in Fig. 1). The magnetization starts out at the value indicated by the large center-dot circle, after which the field is swept down to $\mu_0 H < 29$ T followed by an upsweep to $\mu_0 H > 30$ T.

$\lambda E_Z = 4\Psi^2 \lambda / \pi e \hbar v_F \approx 3$ meV for $2\Psi = 1$ meV, which is comparable to the saturation observed in pulsed magnetic field studies.[24,38]

Should normal scattering processes be inhibited according to the screening model described in the Appendix, Zener tunneling would provide a natural means for the decay of the currents, given the potentially large values of the electric field concentrated close to the sample edge.

IV. MAGNETIC TORQUE MEASUREMENTS

The Hall potential associated with free currents $\mathbf{j}_{free}$ becomes difficult to detect for magnetic-field sweep rates much less than 0.5 T s^{-1}. In contrast, magnetic currents $\mathbf{j}_{mag}$ continue to be present for an arbitrarily long period of time after the magnetic-field sweep is stopped.[12] Figure 9 shows examples of the magnetization of α-(BEDT-TTF)$_2 M$Hg(SCN)$_4$ (for $M=$K and Rb) estimated from the magnetic torque. Magnetic fields of $\mu_0 H \approx 23$ T and $\mu_0 H \approx 32$ T are required to access the CDW_x phase for $M=$K and Rb, respectively;[30] in this phase, hysteresis similar to that originally obtained by Christ *et al.*[12,39] is observed.

The magnetization $\mathbf{M}$ of quasi-two-dimensional metals such as α-(BEDT-TTF)$_2$KHg(SCN)$_4$ is largely directed normal to the conducting layers. A torque $\tau = \frac{1}{2}\mu_0 M_z H \sin 2\theta$ per unit volume therefore occurs when there is a finite angle θ between $\mathbf{M}$ and the applied field $\mathbf{H}$.[30] Sawtoothlike de Haas-van Alphen oscillations (originating from the closed section of Fermi surface that survives CDW formation[30]) account for the larger, reversible contribution to $\mathbf{M}$. These oscillations occur in all metals with closed sections of Fermi surface at low temperatures and result from changes in the equilibrium populations of orbitally quantized Landau levels as H is swept.[40–42] The wave form of the oscillations in the $M=$K salt at high magnetic fields has received much theoretical attention and is well understood.[41,42]

By contrast, the contribution which we attribute to $\mathbf{j}_{mag}$ is irreversible, and depends on how the sample is driven to a particular field and temperature. An example of this is shown in the inset to Fig. 9; if the sample is cooled to 0.5 K at fixed field, the magnetization attains the value surrounded by the circle. On sweeping the field down for the first time, the magnetization rises to meet the path which will be followed by subsequent downsweeps. Moreover, it proves to be impossible to go back to the encircled value of $\mathbf{M}$ by merely changing the field; data recorded on subsequent upsweeps fall below it, while down-sweep data lie above it (Fig. 9, inset). One can only recapture the field-cooled value by warming the sample well above the CDW_x phase and cooling again in the presence of a steady field.

Thus, sweeping the field produces an irreversible contribution to the magnetization that manifests itself as an offset $2\Delta M$ between rising and falling field data in Fig. 9. Figure 10 shows ΔM for a α-(BEDT-TTF)$_2$KHg(SCN)$_4$ sample; values have been extracted by subtracting the reversible de Haas-van Alphen effect contribution (obtained by averaging full up and down sweeps) from the raw magnetization data to leave just the irreversible component. The magnetic field in Fig. 10(a) is first swept slowly up to 29.34 T, then down to 29.24 T, after which the up sweep is resumed. Each time the magnetic-field sweep direction is reversed, a finite interval in field $\Delta H > 2H^*$ (where H^* is the coercion field) is required in order for ΔM to reach a saturation value that opposes the direction of sweep.

The Appendix describes how the CDW system produces a diamagnetic contribution to the magnetization that acts to partially screen the applied magnetic field [see Eq. (A14) and the discussion following it]. However, this contribution saturates when the force on the CDW, $\mathbf{F}$, resulting from a spatially varying free energy, exceeds the pinning force $\mathbf{F}_p$. Elastic energy considerations (see the Appendix) show that the region in which $|\mathbf{F}| > |\mathbf{F}_p|$ propagates inwards from the sample surface as the magnetic field changes, so that the volume fraction of the sample able to contribute to the diamagnetic screening decreases. This is analogous to the scenario in the Bean model of type-II superconductors,[32,43,44] yielding, under the approximation of a cylindrical sample, an irreversible susceptibility

$$\Delta\chi \equiv \frac{\partial \Delta M}{\partial H} = \Delta\chi_0 f(\Delta H) = \Delta\chi_0 \left[1 - \frac{\Delta H}{2H^*}\right]^2 \qquad (16)$$

and an irreversible magnetization

$$\Delta M = \left(\Delta\chi_0 \frac{H^*}{3}\right)\left(2\left[1 - \frac{\Delta H}{2H^*}\right]^3 - 1\right). \qquad (17)$$

Figure 10(b) shows the predicted behavior of the irreversible component of M according to Eq. (17), and Fig. 10(a) shows

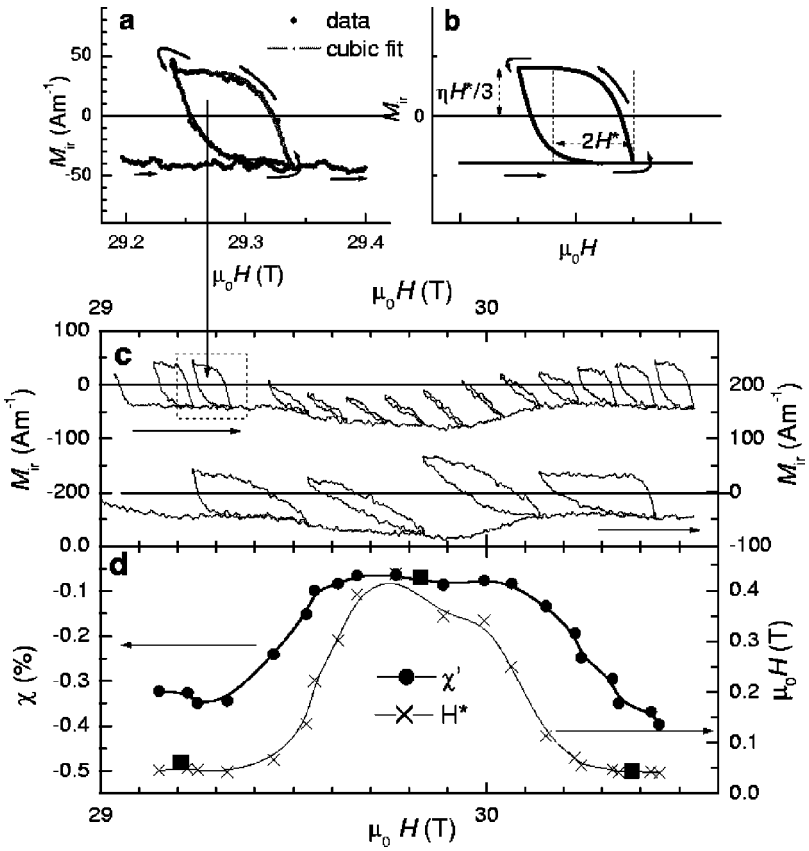

FIG. 10. Evidence for persistent currents in α-(BEDT-TTF)$_2$KHg(SCN)$_4$. (a) An example of a loop in the nonequilibrium component of the magnetization ΔM measured as the field is swept up to 29.33 T then momentarily down to 29.24 T before being resumed. Arrows indicate the change in the locus of ΔM vs H. The solid lines show the results of fits of ΔM to Eq. (17). (b) A model hysteresis loop calculated according to Eq. (17) [i.e., the Bean model for a long cylinder with its axis parallel to H (Refs. 43,44)], showing the theoretical saturation value of ΔM_z and the reversal state. (c) A series of ΔM vs H loops like that in (a) measured over an extended interval of field (top), and (bottom), a similar measurement but where the field interval over which the sweep direction is reversed is increased. Arrows indicate the appropriate axes. (d) Estimates of $\Delta\chi$ from fits of Eq. (17) to the many loops shown in (c) (full circles) together with those (large full squares) calculated according to Eq. (A14) (see also Ref. 32). Estimates of the coercion field H^* (x symbols) are also shown. Arrows indicate the appropriate axes.

a fit of the model to the experimental data. The fact that Eq. (17) reproduces the experimental result indicates that the volume fraction of the sample $f(\Delta H)$ that is able to respond with an irreversible susceptibility $\Delta\chi_0$ declines in a simple quadratic manner with ΔH [see Eq. (16)], behavior typical of critical-state models such as that of Bean;[32,43,44] here, $f(\Delta H)$ is the cross-sectional area of the remaining noncritical portion of the sample.

As the magnetization varies throughout the sample, Maxwell's relation $\mathbf{j}_{\mathrm{mag}}=\boldsymbol{\nabla}\times\mathbf{M}$ (Ref. 31) implies that a magnetic-field-induced critical state always involves currents. However, although a critical-state model provides an excellent fit to the experimental data in Fig. 10(a), it is important to note that there are two essential properties of the currents giving rise to the loops in Fig. 10 that distinguish them from those in superconductors. First, the magnitude of the nonequilibrium susceptibility $|\Delta\chi_0|\approx 3\times 10^{-3}$ (obtained from the fits) departs significantly from the ideal diamagnetic value $\Delta\chi_0\approx -1$ observed in superconductors. This implies that the magnetic currents in α-(BEDT-TTF)$_2M$Hg(SCN)$_4$ cannot be considered as screening currents in the same sense as those in superconductors. Because the magnetic currents screen only a part of the magnetic field, the effective coercion field $H^*\approx j_c r_0/\Delta\chi_0$ is rather large. Second, the value of $\Delta\chi_0$ varies strongly as a function of H in Figs. 10(c) and 10(d), a property that would be very difficult to explain in terms of superconductivity, but which is an intrinsic feature of the model of a CDW coexisting with well-defined Landau levels discussed in the Appendix.

Figure 10(c) shows a series of loops in ΔM_z versus H like that in (a), from which $\Delta\chi_0$ is extracted at various values of H in (d). The magnitude of $\Delta\chi_0$ is low and of the order of 5×10^{-4} when μ is situated in the middle of a Landau level (at half-integral filling factors), but increases almost tenfold when μ is between Landau levels (at integral filling factors). The theoretical limit for $\Delta\chi_0$ becomes equivalent to that of a superconductor (i.e., $\Delta\chi_0=-1$) only in that case of an ideal sample at integral filling factors in which the quantum lifetime is infinite [see Eq. (A14) in the Appendix, remembering that demagnetizing factors[31] must be taken into account once the susceptibility becomes very large].

When pinning of the CDW occurs, the nonequilibrium susceptibility $\Delta\chi_0$ provides a measure of how quickly the CDW departs from equilibrium as the magnetic field is swept. This occurs more rapidly at integral Landau-level filling factors where the density of states is lowest, enabling μ to jump quickly between Landau levels.[32] Pinning of the CDW prevents the equilibrium redistribution of carriers between the bands, causing this jump to become much more abrupt. This can account the origin of the strong variations in $\Delta\chi_0$ in Fig. 10(d), as shown by the model calculations (see the Appendix).

V. DISCUSSION AND CONCLUSION

Before concluding this paper, it is instructive to compare effective ac susceptibilities of α-(BEDT-TTF)$_2$KHg(SCN)$_4$ determined using different methods in Fig. 11. In Fig. 11(a), $\chi'\equiv\Delta\chi_0$ is obtained by fitting the Bean model [as described above—see Eq. (17)] to many hysteresis loops over an ex-

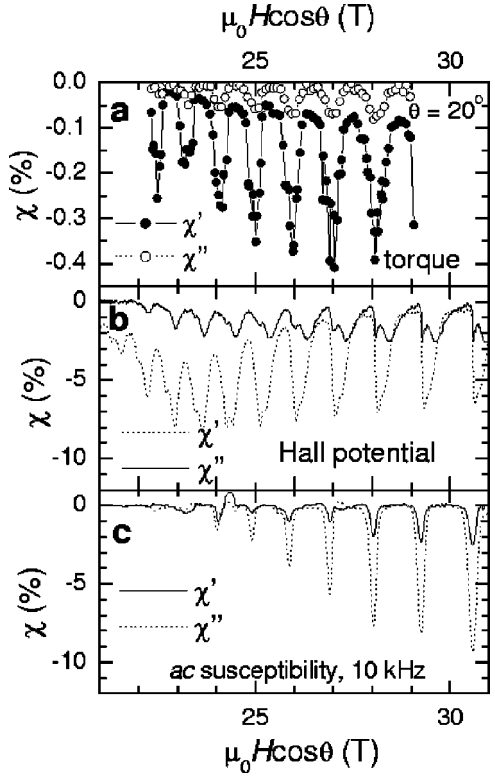

FIG. 11. A comparison of ac susceptibilities (or equivalent ac susceptibilities) made on α-(BEDT-TTF)$_2$KHg(SCN)$_4$ using different methods. In (a) this is determined by fitting Eq. (17) to many hysteresis loops over an extended interval in magnetic field. The imaginary component is determined from the area of the loop divided by its width. In (b), the effective susceptibility is obtained by equating $\chi' = 2\pi V''_{\rm H}/\rho_{xy}\mu_0\tilde{H}$, where $V''_{\rm H}$ is the reactive component of the Hall potential. The imaginary susceptibility is given by $\chi' = 2\pi V'_{\rm H}/\rho_{xy}\mu_0\tilde{H}$. Here, the susceptibility is estimated from the data in Fig. 3. (c) is the published ac susceptibility measured on another sample (Ref. 33).

tended region of magnetic field. The imaginary component χ'', which accounts for losses, is obtained from the loop areas. In Fig. 11(b), the susceptibility is estimated using

$$\chi' - i\chi'' = \frac{-2\pi i}{\rho_{xy}\tilde{H}}(V'_{\rm H} - iV''_{\rm H}). \tag{18}$$

The most clear aspect of Fig. 11 is that the magnitudes of the real and imaginary susceptibilities due to free currents $\mathbf{j}_{\rm free}$, estimated from the ac Hall potential, agree more closely with the high-frequency ac susceptibility measurements made in Ref. 33 [shown in Fig. 11(c)] than with the magnetic torque measurements. This indicates that the ac susceptibility made at frequencies $\omega/2\pi \gtrsim 50$ Hz consists mostly of free currents $\mathbf{j}_{\rm free}$, which are shown (above, and in the Appendix) to be confined to the sample edges. The data in Fig. 8 shows that $\mathbf{j}_{\rm free}$ can persist for times as long as $t_0^{\rm decay} \gtrsim 0.5$ ms for sufficiently small values of the Hall potential $V_{\rm H} \lesssim 7$ μV in a sample of ~ 1 mm^2 cross section at $\mu_0 H \approx 25$ T and $T \approx 0.5$ K. In spite of the fact that the corresponding susceptibility in Fig. 11(b) is much larger than that for the torque measurements in Fig. 11(a), the magnetization $M_{\rm free} = V_{\rm H}/\rho_{xy} \approx 7$ Am^{-1} due to free currents is actually smaller. Free currents therefore have insufficient duration to contribute a significant amount to the irreversible steady magnetic torque in Fig. 10. By contrast, magnetic currents observed in the torque experiments last for an indefinite period of time.[12]

The combined induction of free and magnetic currents $\mathbf{j}_{\rm free} + \mathbf{j}_{\rm mag}$ can therefore be understood as follows: for small changes in magnetic field $\mu_0 \Delta H \ll 10$ mT, the greatest contribution to the susceptibility initially originates from free currents at the surface that attempt to screen changes in magnetic flux density from within the bulk. These currents quickly saturate, however, as dissipation sets in, possibly assisted by Zener tunneling. At that point, changes in magnetic flux density enter the bulk which cause the Landau level structure and chemical potential to change, causing the CDW to depart from equilibrium, as described in the Appendix. The stored energy increases quadratically with ΔH, eventually causing the CDW to collapse at the edges, initiating the critical state.

In conclusion, Hall potential and magnetic torque measurements on α-(BEDT-TTF)$_2M$Hg(SCN)$_4$ (M=K, Rb) show that two types of screening currents occur within the high-field, low-temperature CDW$_x$ phase in response to changing magnetic fields. The first, which gives rise to the induced Hall potential, is a free current ($\mathbf{j}_{\rm free}$), weighted mostly towards the edge of the sample. The time constant for the decay of these currents is longer than that expected from the sample resistivity. The second component of the current appears to be magnetic ($\mathbf{j}_{\rm mag}$), in that it is a microscopic, quasiorbital bulk effect; it is evenly distributed within the sample upon saturation. A simple model (Appendix), describing a new type of quantum fluid comprising a CDW coexisting with a two-dimensional Fermi-surface pocket, is able to account for the origins of the currents. Taken together, these findings are able to reconcile the body of experimental evidence[12,20–27] which had previously been interpreted in terms of the quantum Hall effect[30] or superconductivity.[25]

ACKNOWLEDGMENTS

This work was supported by U.S. Department of Energy (DOE) under Grant No. LDRD-DR 20030084 and by the UK Engineering and Physical Sciences Research Council (EPSRC). The National High Magnetic Field Laboratory was supported by DOE, the National Science Foundation (NSF), and the State of Florida. We thank Stan Tozer and Alessandro Narduzzo for experimental assistance, and acknowledge stimulating discussions with James Brooks, Jason Lashley, and Albert Migliori.

APPENDIX: SCREENING MECHANISMS IN α-(BEDT-TTF)$_2$KHg(SCN)$_4$

We treat a simplified version of the α-(BEDT-TTF)$_2$KHg(SCN)$_4$ band structure,[30] comprising a 1D electron band and a two-dimensional(2D) hole band with dispersions $\varepsilon_{1D} = \hbar v_{\rm F}|k_x - k_{\rm F}|$ and $\varepsilon_{2D} = \varepsilon_{\rm F} - \hbar^2(|k_x - k_X|^2$

$+|k_y-k_Y|^2)/2m$, respectively; here m is the effective mass, v_F is the Fermi velocity of the 1D band, and k_X and k_Y define the center of the 2D hole pocket. Each of these bands intersects the Fermi energy (ε_F), giving rise to the simplified Fermi surface shown in the inset to Fig. 2.

The simplest scenario to consider is that where only the 1D Fermi-surface section is subject to CDW formation, giving rise to a gap 2Ψ in its density of electronic states, while the 2D hole section remains ungapped. Under equilibrium conditions, the average volume charge densities $\bar{\varrho}_{1D}$ and $\bar{\varrho}_{2D}$ associated with the 1D and 2D Fermi-surface sections, respectively, would be subject to the conservation equation $\bar{\varrho}_{1D}+\bar{\varrho}_{2D}+\varrho_{bg}=0$, where ϱ_{bg} is the density of charge due to the ionic cores. However, below we consider slight local deviations $\Delta\varrho_{1D}$ and $\Delta\varrho_{2D}$ in the charge density from the equilibrium values (i.e., the total local charge densities associated with the 1D and 2D Fermi-surface sections become $\varrho_{1D}=\Delta\varrho_{1D}+\bar{\varrho}_{1D}$ and $\varrho_{2D}=\Delta\varrho_{2D}+\bar{\varrho}_{2D}$, respectively); because of the presence of the CDW, the overall conservation equation need no longer hold *locally*. However, the charge densities must obey Poisson's equation

$$-\epsilon\nabla^2 V(\mathbf{r})=\Delta\varrho_{2D}+\Delta\varrho_{1D}, \tag{A1}$$

where V is the electrostatic potential and ϵ is the permittivity. We are at liberty to set the origin of potential; we choose $V=0$ in the absence of spatial charge variations. Equation (A1) implies that the presence of local charge-density variations will lead to an in-plane, spatially varying electric field $\mathbf{E}=-\nabla V$.

We now introduce the magnetic-flux density $\mathbf{B}_0$ applied along z [i.e., $\mathbf{B}=(0,0,B)\equiv B\hat{\mathbf{z}}$, $\perp$ to the 2D (x,y) planes]. This has two effects; first, the crossed $\mathbf{E}$ and $\mathbf{B}$ fields force the 2D hole wave function centers to drift at a velocity $\mathbf{E}\times\mathbf{B}_0/B_0^2$. This leads to a spatially varying in-plane current density, which, provided that the scattering rate is rather small (e.g., under conditions of ballistic or quasiballistic transport), can be written as $\mathbf{j}\approx\varrho_{2D}\mathbf{E}\times\mathbf{B}_0/B_0^2$; note that the relationship becomes exact in the total absence of scattering. Integration of Maxwell's fourth equation ($\nabla\times\mathbf{H}=\mathbf{j}$[31]) shows that this current produces an additional contribution

$$\Delta\mathbf{B}=-\mu_0\varrho_{2D}(V/B_0)\hat{\mathbf{z}} \tag{A2}$$

to the magnetic-flux density parallel to z, which then becomes $\mathbf{B}=\mathbf{B}_0+\Delta\mathbf{B}$. A second effect of $\mathbf{B}$ is to produce Landau quantization of the 2D holes; this is usually dealt with using the Landau gauge $\mathbf{A}=(0,Bx,0)$.[45] After some manipulation,[45] the Schrödinger equation for the in-plane wave functions ψ and eigenenergies E may be written as

$$\left(-\frac{\hbar^2}{2m}\frac{\partial^2}{\partial x^2}+\frac{1}{2}m\omega_c^2(x-x_0)^2\right)\psi=E\psi.$$

Here, the effect of the crystalline potential has been taken into account by the effective mass m, the cyclotron frequency is $\omega_c=qB/m$, with q the charge; x_0 represents the wave function guiding-center coordinate.

The in-plane electric field also modifies the Landau-level energies.[36] To quantify this, we consider the case $V(\mathbf{r})=V(x)$, i.e., the potential varies only in the x direction (variation in an arbitrary direction in the x,y plane is reintroduced below). If $V(x)$ varies slowly over length scales $\sim x_0$, it can be expanded about x_0 in a Taylor's series $V(x)=V(x_0)+(x-x_0)V'(x-x_0)+\frac{1}{2}(x-x_0)^2V''(x_0)+\cdots$, where the primes indicate differentiation with respect to x. After a little algebra, the Schrödinger equation becomes

$$-\frac{\hbar^2}{2m}\frac{d^2\psi}{dx^2}+\left[\frac{1}{2}m\left(\omega_c^2+\frac{q}{m}V''(x_0)\right)(x-x_1)^2\right]\psi=E\psi, \tag{A3}$$

where x_1 is a constant [absorbing terms in x_0, $V(x_0)$ and $V'(x_0)$].

The chief effect of $V(x)$ comes from $V''(x_0)$; this gives a modified Landau-level spectrum, $(n+\frac{1}{2})\hbar\omega$, with n an integer and

$$\omega=\omega_c\left(1+\frac{qV''}{2m\omega_c^2}\right)^{1/2}\approx\omega_{c0}\left(1+\frac{\Delta B}{B_0}+\frac{V''}{2\omega_{c0}B_0}\right), \tag{A4}$$

where $\omega_{c0}=qB_0/m$ and only terms to leading order in ΔB and V'' are retained in the right-hand bracket. Reintroducing a potential variation in an arbitrary intraplane direction merely changes V'' in Eq. (A4) to ∇^2V.

In the absence of potential variations, the number of states per unit volume per Landau level is $D=D_0=m\omega_{c0}/\pi\hbar c$, where c is the layer separation in the z direction; the introduction of varying V (and consequent $\Delta\mathbf{B}$) causes ω_{c0} to change to ω [Eq. (A4)], modifying this to $D=m\omega/\pi\hbar c=D_0+\Delta D$, where

$$\Delta D=D_0\left(\frac{\Delta B}{B_0}+\frac{\nabla^2V}{2\omega_{c0}B_0}\right). \tag{A5}$$

The change in Landau-level degeneracy results in a change to the local 2D hole density,

$$\Delta\varrho_{2D}=\nu q\Delta D-\nu\beta q\Delta D-\beta q\bar{g}_{2D}\Delta\mu. \tag{A6}$$

It is worth taking time to understand this equation fully, since it is the key to understand the screening effects that are the point of this paper. The first term of the right-hand side results from the change in degeneracy of *all* of the occupied Landau levels; positive $\nabla^2V(\mathbf{r})$ or $\Delta\mathbf{B}$ gives a greater Landau-level degeneracy [Eq. (A5)], producing an *increase* in the number of holes. The second term results from the energy shift of the νth Landau level closest to the chemical potential μ; in the high-field limit of well-resolved levels, the contribution from the tails of the Landau-levels remote from μ can be ignored. As an increase in $\nabla^2V(\mathbf{r})$ causes ω to increase [Eq. (A4)], this results in a slight *depopulation* of the Landau levels closest to μ, acting to reduce ϱ_{2D}. The dimensionless factor β therefore depends critically on the position of μ amongst the Landau levels, i.e., it oscillates as a function of B. If μ is in the middle of the highest occupied Landau level (at half-integral Landau-level filling, $\nu=F/B$), the density of states is large, so that the shift in energy of the Landau level has a relatively large effect on ϱ_{2D}; in this

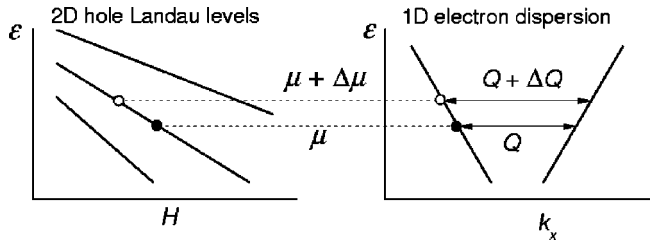

FIG. 12. A model depicting the effect of a change $\Delta\mu \propto \Delta N_{1D}$ in the chemical potential μ on the 2D hole Landau levels and the 1D electron dispersions (in this case at half-integer filling), giving rise to a direct relationship between ΔN_{1D}, $\Delta\mu$, and ΔQ and consequently between ΔQ and H.

situation, $\beta_{\rm half} \approx 2\omega_c\tau/\pi \gg 1$. On the other hand, if μ is directly between two Landau levels (at integral Landau-level filling $\nu = F/B$) then the density of states is small and $\beta_{\rm int} \approx 4/\pi\omega_c\tau \ll 1$. This tends to zero in the case of a sample of pristine purity for which the quantum lifetime $\tau \to \infty$.[36] The final term accounts for possible spatial variations $\Delta\mu$ in the chemical potential which are sustained by the CDW (see below); here, $\overline{g}_{2D} \equiv \overline{\varrho}_{2D} m/\hbar F q^2$ is the mean value of the 2D density of states.

A shift in the chemical potential also affects the 1D carrier density;

$$\Delta\varrho_{1D} = -\gamma e g_{1D} \Delta\mu, \tag{A7}$$

where g_{1D} is the 1D density of states and $\gamma = 1$ provided the CDW is in equilibrium.[32] We can now reformulate Eq. (A6) by substituting from Eqs. (A1), (A2), (A5), and (A7) to yield

$$\frac{1}{2\omega_{c0}} \nabla^2 V + \Delta B = \frac{m}{\hbar e \nu} \left(\frac{\beta + \gamma\eta}{1-\beta} \right) \Delta\mu. \tag{A8}$$

We have retained terms up to first order in small quantities, omitted $\epsilon \nabla^2 V$ from Eq. (A1) because it is $\sim 10^4$ times smaller than the other term in $\nabla^2 V$ and substituted $q = +e$ for the hole charge;[46] here, $\eta = g_{1D}/g_{2D}$.

As long as the 1D band remains metallic, $\Delta\mu$ is unconstrained. Scattering facilitates the transfer of current between positive and negative variations in the charge density, causing them to dissipate rapidly. The stable result is when $\nabla^2 V = 0$, causing Eq. (A8) to become a simple proportionality between $\Delta\mu$ and ΔB; i.e., a variation in the chemical potential due to a change in magnetic field.[42]

By forming a CDW on the 1D bands, the system can benefit in two ways. First, by the opening of a CDW gap 2Ψ, the system has the potential to become partly gapped at μ. Second, by forming a quantum-coherent state, the 1D band resists the spontaneous exchange of charge between the two bands. As with a superconductor, the quantum state of a CDW is locally defined by a phase ϕ, which defines the phase of the charge modulation that oscillates in one direction (x) on a length scale $2\pi/|\mathbf{Q}|$ much shorter than the cyclotron length. Any shift in the chemical potential in Eq. (A8) will correspond to a gradient in phase (see Fig. 12),

$$\Delta\mu = \frac{\hbar v_F}{2} \frac{\partial\phi}{\partial x}. \tag{A9}$$

The proportionality between $\partial\phi/\partial x$ and $\Delta\mu$ leads to two qualitatively different solutions to Eq. (A8).

1. Within the bulk of the sample

In the bulk of the sample, the transport is dissipative ($\nabla^2 V \to 0$) and the equilibrium phase of the CDW becomes dependent only on the magnetic field. Equation (A8) therefore becomes

$$\frac{\Delta\mu}{\Delta B} = \frac{\hbar e \nu}{m} \left(\frac{1-\beta}{\beta + \gamma\eta} \right). \tag{A10}$$

Thus, there is a direct proportionality between local variations in the magnetic field and $\Delta\mu$.

A nonequilibrium $\Delta\tilde{\mu}$ will develop, however, if the phase is unable to relax to the equilibrium value due to the effect of pinning in the bulk; here, and in the discussion that follows we will represent such nonequilibrium quantities using a tilde ($\sim$). A fully pinned CDW is unable to exchange charge with the 2D Landau levels,[32] causing $\gamma \to 0$ in Eq. (A7). A nonequilibrium change $\Delta\tilde{\mu}$ results in a nonequilibrium shift in the CDW phase [Eq. (A9)], and, via[32]

$$\frac{\partial \Delta\tilde{Q}}{\partial \Delta\tilde{\mu}} = \overline{Q} \frac{g_{1D} e}{|\varrho_{1D}|} \tag{A11}$$

to local adjustments of Q away from its equilibrium value, $\overline{Q}$ (see Fig. 12). These changes result in a concomitant shift in the free energy Φ of the system, which, following Ref. 32, can be written as

$$\Phi = -g_{1D} \left(\frac{\Psi^2}{2} - \Delta\tilde{\mu}^2 \right) + \delta g_{1D} \Delta\tilde{\mu}^2 + \Phi_{2D}(\varrho_{1D}). \tag{A12}$$

Here, Φ_{2D} is the free energy of the Landau-level system (which depends at fixed field on the number of quasiparticles in the 2D hole band, and hence on ϱ_{1D}) and δ is a dimensionless parameter depending on the position of the chemical potential amongst the Landau levels; it takes the limiting values[32]

$$\delta = \frac{1}{2\eta \frac{\pi}{4} \omega_c\tau} - \frac{1+\eta}{2\left(\eta \frac{\pi}{4} \omega_c\tau \right)^2} \tag{A13}$$

for integer Landau-level filling factors and $\delta = \frac{1}{2}$ for half-integer filling factors.

The effects described by Eqs. (A10)–(A12) result in a relationship between Φ and ΔB, implying that there is a contribution $\Delta\chi$ from the CDW to the overall susceptibility χ, where $\Delta\chi \equiv -\mu_0 (\partial^2\Phi/\partial(\Delta B)^2)$. Using the identity $(\partial\Phi/\partial(\Delta B)) = (\partial\Phi/\partial(\Delta\tilde{\mu})) \times (\partial(\Delta\tilde{\mu})/\partial(\Delta B))$ in conjunction with Eqs. (A10) and (A12) yields[47]

$$\Delta\chi = -2 g_{1D} \mu_0 (1+\delta) \left[\frac{\hbar e \nu}{m} \left(\frac{1-\beta}{\beta} \right) \right]^2. \tag{A14}$$

Thus, the nonequilibrium (i.e., spatially varying) state of the CDW provides a diamagnetic contribution to the overall susceptibility, which resists changes in the magnetic field in the bulk of the sample; note that the presence of the factors β and δ indicate that the effectiveness of this screening will oscillate as a function of Landau-level filling factor ν. However, as we discuss in the next paragraph, Eq. (A14) represents the response of the sample only to infinitesimal changes in magnetic field; the build up (and release) of elastic energy as the field develops further leads to an irreversible change in the overall sample susceptibility which eventually saturates.

The spatially varying free energy associated with the mechanism causing Eq. (A14) corresponds to a force $\mathbf{F}=-\nabla\Phi$; the nonequilibrium excited state of the CDW will only persist if $\mathbf{F}$ remains less than the CDW's pinning force $\mathbf{F}_p$.[32] This produces two restrictions; first, because of the differential relationship between $\mathbf{F}$ and $\Delta\tilde{\mu}$, $\Delta\tilde{\mu}$ must tend to zero at the sample surface, or else $\mathbf{F}$ would be singular (and hence exceed $\mathbf{F}_p$). Second, once $\mathbf{F}$ develops with changing field to such an extent that the CDW depins, the nonequilibrium buildup of $\Delta\tilde{\mu}$ must stop, preventing any further contribution from $\Delta\chi$. These combine to ensure that the region in which $|\mathbf{F}|>|\mathbf{F}_p|$ propagates inwards from the sample surface as the magnetic field changes, so that the volume fraction of the sample able to contribute $\Delta\chi$ [Eq. (A14)] to the overall volume-averaged sample susceptibility χ becomes progressively smaller. This is very similar to the Bean critical-state model;[32,43,44] indeed, a common feature of *all* critical-state models is that motion initiates at the surface because it is there that the potential energy can be dissipated with the least amount of action. The CDW begins to slide at the sample surface so that the restoring force does not exceed the CDW depinning force. Approximately linear gradients in $\Delta\varrho_{1D}$ and $\Delta\tilde{Q}$ occur because the work done by $\mathbf{F}$ is a linear function of the departure $\Delta\tilde{Q}$ of the CDW from equilibrium.[32] Currents result from changes in the charge density ϱ_{2D} associated with the two-dimensional Fermi surface section as the quasiparticles redistribute themselves so as to screen the changes in the open Fermi surface section [see Eq. (A1)]. The variation in the orbital magnetization of the closed Fermi-surface pocket ΔM with $\Delta\varrho_{2D}$ then leads to linear gradients in ΔM. Maxwell's equations imply that a linear gradient in ΔM, sustained by pinning, corresponds to a critical current density $\mathbf{j}_c=\nabla\times(\Delta\mathbf{M})$, in the region where the CDW is able to slide.

Therefore, although the mechanisms are very different, there are close analogies between the situation here and flux pinning in superconductors. It is therefore not surprizing that in Sec. IV, we shall see that a simple Bean model is able to fit the variation of sample susceptibility with applied magnetic field.

2. Close to the sample surface

We have already seen that $\Delta\tilde{\mu}\rightarrow 0$ as one approaches the sample surface because the elastic energy cost of shifting the phase would otherwise become too great. Hence, Eq. (A8) assumes the form

$$\lambda^2\nabla^2 V - V = 0 \quad \text{with} \quad \lambda=[m/(2\mu_0 e\bar{\varrho}_{2D})]^{1/2}, \tag{A15}$$

where we have substituted for ΔB using Eq. (A2). Equation (A15) defines a penetration depth λ analogous to the London penetration depth in superconductivity; it implies that deviations V from the equilibrium value of the electrostatic potential will be screened from the bulk of the sample. Owing to the proportionality between V and ΔB in Eq. (A2), spatial variations in the magnetic field will also be screened. Substituting values for α-(BEDT-TTF)$_2$KHg(SCN)$_4$ taken from Ref. 30 yields $\lambda\approx 400$ nm.

The existence of a finite $\nabla^2 V$ close to the surface implies quasiballistic transport. By carrying the current close to the edges, the total system can save energy (in this case, elastic energy due to the nonequilibrium arrangement of the CDW within the bulk of the sample), and any process that saves energy also protects the quasiparticles from ordinary scattering events that would otherwise give rise to dissipative bulk currents. This type of explanation for the variation in the current density, electrostatic potential, electric field, and perturbed charge carrier density follows on from a model originally proposed by MacDonald *et al.*[36] for two-dimensional electron gas systems. Whereas for a single two-dimensional layer an exact solution can only be obtained numerically, in bulk crystalline systems like α-(BEDT-TTF)$_2$KHg(SCN)$_4$, the above treatment shows that the variation in all of these quantities becomes a simple exponential function.

[1] G. Grüner, Rev. Mod. Phys. **60**, 1129 (1988).

[2] G. Grüner, *Density Waves in Solids*, Frontiers in Physics Vol. 89 (Addison-Wesley, Reading, MA, 1994).

[3] J. Sólyom, Adv. Phys. **28**, 201 (1979).

[4] W. Dietrich and P. Fulde, Z. Phys. **265**, 239 (1973).

[5] D. Zanchi, A. Bjeliš, and G. Montambaux, Phys. Rev. B **53**, 1240 (1996).

[6] R.H. McKenzie, cond-mat/9706235 (unpublished).

[7] N. Harrison, Phys. Rev. Lett. **83**, 1395 (1999).

[8] This situation contrasts with that in superconductors, where phenomena associated with the Pauli limit are accessible to laboratory fields: see, e.g., J. Singleton, J.A. Symington, M.-S. Nam, A. Ardavan, M. Kurmoo, and P. Day, J. Phys.: Condens. Matter, **12**, L641 (2000); H. Won, K. Maki, S. Haas, N. Oeschler, F. Weickert, and P. Gegenwart, cond-mat/0306548 (unpublished). In superconductors, the characteristic energy scale that defines the transition temperature is Debye frequency of the phonons, whereas in CDW systems it is the total electronic bandwith (Refs. 1,2).

[9] P. Foury-Leylekian, S. Ravy, J.P. Pouget, and H. Muller, Synth. Met. **137**, 1271 (2003).

[10] N. Biskup, J.A.A.J. Perenboom, J.S. Brooks, and J.S. Qualls,

Solid State Commun. **107**, 503 (1998).
[11] P. Christ, W. Biberacher, M.V. Kartsovnik, E. Steep, E. Balthes, H. Weiss, and H. Müller, JETP Lett. **71**, 303 (2000).
[12] N. Harrison, L. Balicas, J.S. Brooks, and M. Tokumoto, Phys. Rev. B **62**, 14 212 (2000).
[13] N. Harrison, E. Rzepniewski, J. Singleton, P.J. Gee, M.M. Honold, P. Day, and M. Kurmoo, J. Phys.: Condens. Matter **11**, 7227 (1999).
[14] M. Oshima, H. Mori, G. Saito, and K. Oshima, Chem. Lett. **7**, 1159 (1989); H. Mori, S. Tanaka, M. Oshima, G. Saito, T. Mori, Y. Maruyama, and H. Inokuchi, Bull. Chem. Soc. Jpn. **63**, 2183 (1990).
[15] M.V. Kartsovnik, A.E. Kovalev, and N.D. Kushch, J. Phys. I **3**, 1187 (1993).
[16] S. Uji, T. Terashima, H. Aoki, J.S. Brooks, M. Tokumoto, N. Kinoshita, T. Kinoshita, Y. Tanaka, and H. Anzai, Phys. Rev. B **54**, 9332 (1996).
[17] N. Harrison, L. Balicas, J.S. Brooks, J. Sarrao, and Z. Fisk, Phys. Rev. B **61**, 14 299 (2000).
[18] N. Harrison, N. Biskup, J.S. Brooks, L. Balicas, and M. Tokumoto, Phys. Rev. B **63**, 195102 (2001).
[19] D. Andres, M.V. Kartsovnik, W. Biberacher, H. Weiss, E. Balthes, H. Müller, N. Kushch, Phys. Rev. B **64**, 161104 (2001).
[20] N. Harrison, A. House, M.V. Kartsovnik, A.V. Polisski, J. Singleton, F. Herlach, W. Hayes, and N.D. Kushch, Phys. Rev. Lett. **77**, 1576 (1996).
[21] S. Hill, P.S. Sandhu, J.S. Qualls, J.S. Brooks, M. Tokumoto, N. Kinoshita, T. Kinoshita, and Y. Tanaka, Phys. Rev. B **55**, R4891 (1997).
[22] N. Harrison, M.M. Honold, M.V. Kartsovnik, J. Singleton, S.T. Hannahs, D.G. Rickel, and N.D. Kushch, Phys. Rev. B **55**, 16 005 (1997).
[23] M.M. Honold, N. Harrison, J. Singleton, H. Yaguchi, C.H. Mielke, D. Rickel, I. Deckers, P.H.P. Reinders, F. Herlach, M. Kurmoo, and P. Day, J. Phys.: Condens. Matter **9**, L533 (1997).
[24] M.M. Honold, N. Harrison, J. Singleton, M.-S. Nam, S.J. Blundell, C.H. Mielke, M.V. Kartsovnik, and N.D. Kushch, Phys. Rev. B **59**, R10 417 (1999).
[25] N. Harrison, C.H. Mielke, J. Singleton, J.S. Brooks, and M. Tokumoto, J. Phys.: Condens. Matter **13**, L389 (2001).
[26] N. Harrison, Int. J. Mod. Phys. B **16**, 3072 (2002).
[27] C.H. Mielke, N. Harrison, A. Ardavan, P. Goddard, J. Singleton, A. Narduzzo, L.K. Montgomery, L. Balicas, J.S. Brooks, and M. Tokumoto, Synth. Met. **133**, 99 (2003).
[28] T. Chakraborty and P. Pietiläinen, *The Quantum Hall Effects: Integral and Fractional*, 2nd ed., Springer Series in Solid-State Sciences Vol. 85 (Springer-Verlag, Berlin, 1995).
[29] M. Tinkham, *Introduction to Superconductivity*, 2nd ed. (McGraw-Hill, New York, 1996).
[30] J. Singleton, Rep. Prog. Phys. **63**, 1111 (2000).
[31] B. I. Bleaney and B. Bleaney, *Electricity and Magnetism*, 3rd ed. (Oxford University Press, Oxford, 1989).
[32] N. Harrison, Phys. Rev. B **66**, 121101(R) (2002).
[33] N. Harrison, C.H. Mielke, A.D. Christianson, J.S. Brooks, and M. Tokumoto, Phys. Rev. Lett. **86**, 1586 (2001).
[34] A.A. Abrikosov, *Fundamentals of the Theory of Metals* (Elsevier Science Publishers, Amsterdam, 1988).
[35] L. Balents and M.P.A. Fisher, Phys. Rev. Lett. **76**, 2782 (1996).
[36] A.H. MacDonald, T.M. Rice, and W.F. Brinkman, Phys. Rev. B **28**, 3648 (1983).
[37] See, e.g., Leigh Page and N.I. Adams, *Principles of Electricity*, 4th ed. (Van Nostrand, Princeton, NJ, 1969), p. 319.
[38] M.M. Honold, N. Harrison, M.V. Kartsovnik, H. Yaguchi, J. Singleton, C.H. Mielke, N.D. Kushch, M. Kurmoo, and P. Day, Phys. Rev. B **62**, 7908 (2000).
[39] P. Christ, W. Biberacher, H. Müller, K. Andres, E. Steep, and A.G.M. Jansen, Physica B **204**, 153 (1995).
[40] D. Shoenberg, *Magnetic Oscillations in Metals* (Cambridge University Press, Cambridge, 1984), pp. 41–53.
[41] M.A. Itskovsky, T. Maniv, and I.D. Vagner, Phys. Rev. B **61**, 14 616 (2000).
[42] N. Harrison, R. Bogaerts, P. Reinders, J. Singleton, S.J. Blundell, and F. Herlach, Phys. Rev. B **54**, 9977 (1996).
[43] C.P. Bean, Rev. Mod. Phys. **36**, 31 (1964).
[44] C.P. Poole, H.A. Farach, and R.J. Creswick, *Superconductivity* (Academic, San Diego, CA, 1995), pp. 371–390.
[45] See, e.g., J. Singleton, *Band Theory and Electronic Properties of Solids* (Oxford University Press, Oxford, UK, 2001), pp. 87–89.
[46] Note that the result depends only on q/m, and so is independent of whether we consider the 2D Fermi surface as a hole pocket with positive m and q or an electron pocket with negative m and q.
[47] Note that this equation is the same as Eq. (4) of Ref. 32.